Sandia National Laboratories is a multimission laboratory managed and operated by National Technology and Engineering Solutions of Sandia, LLC, a wholly owned subsidiary of Honeywell International, Inc., for the U.S. Department of Energy’s National Nuclear Security Administration under contract DE-NA-0003525.

Sandia National Laboratories is a multimission laboratory managed and operated by National Technology & Engineering Solutions of Sandia, LLC, a wholly owned subsidiary of Honeywell International Inc., for the U.S. Department of Energy's National Nuclear Security Administration under contract DE-NA0003525.

LABORATORY DIRECTED RESEARCH & DEVELOPMENT
WHERE INNOVATION BEGINS

SAND21XX-XXXXR
LDRD PROJECT NUMBER: 227334
LDRD PROJECT TITLE: Development of Quantum Computing Interconnect Based on Aerosol Jet Printing and Electrochemical Deposition of Rhenium
PROJECT TEAM MEMBERS: Judi Lavin; Lok-kun Tsui; Qiang Huang; Kamal Ahammed; Emily Weigel.

ABSTRACT:

The electrodeposition of rhenium on to a metal seed layer on flexible substrates is presented as a means to creating superconducting flexible cable connectors in an enabling plug-and-play approach for quantum computing. Cryogenic quantum electronics are currently connected using masses of stainless-steel coaxial cables that are bulky, rigid - both in form and design - and lead to significant joule heating, thermal noise, and cross talk. Here, we present an unprecedented approach to integrate an aerosol jet printed (AJP) metal seed layer with rhenium electrodeposition on a flexible substrate in the advancement of superconducting interconnect technologies. Silver and gold were printed using the 'Nanojet' aerosol jet printer on Kapton films. Adhesion of gold was found to be far superior to that of silver and adhesion on roughened Kapton surpassed that of its smooth counterpart. Electrodeposition of rhenium was successful on both silver and gold and an amorphous Re film was confirmed by XRD. Results for both materials are presented however due to the poor adhesion of silver to Kapton it was ruled out as a viable candidate. Composite materials were characterized by profilometry, EDS, XRD and FIB-SEM. Electrical measurements of the composite at ambient temperature showed a critical temperature (T_c), where the resistance drops to 0, of 5.8 K, well above 4.2 K, the temperature of liquid helium. Stress-strain tests of the Ag-Re and Au-Re composites on roughened and smooth Kapton were completed. Cyclic flexure testing (200 cycles) to 1.25% strain showed smooth Kapton samples reach a stress of ~16 MPa, while Kapton roughened with sandpaper, reaches ~20MPa of stress for the same 1.25% strain.

INTRODUCTION AND EXECUTIVE SUMMARY OF RESULTS:

The need to develop and build quantum computers that are faster, of higher fidelity and more cost effective than existing digital computer technology exists. In quantum computing research where multiple temperature stages down to milli-Kelvin temperatures are required, a large effort exists to limit thermal leakage and minimize joule heating. Superconducting flexible cable connectors are sought after to enable plug-and-play type of assembly for cryogenic electronic devices such as quantum computers and to improve operation fidelity by eliminating thermal

perturbations and reducing thermal noise during power and signal transmission. Current state-of-the-art connectors and cables are made from coaxial stainless steel, which not only require manual assembly of numerous individual cables but also result in significant joule heating during operation. Then, there exists the need for high-density, low loss and low thermal leakage in addition to having a light and flexible modality to work with.

Quantum computers aim to solve a range of limitations which are currently unachievable with conventional computing technology. These applications include physics and chemistry simulations, cryptography, machine learning, medicine, and finance [1-5]. The processing of quantum computers relies on qubits which are implemented with superconducting Josephson junctions cooled to 10 mK by a dilution refrigerator [6]. Connections to the qubits from the outside are achieved with a chandelier of stainless-steel cables that must be connected individually [6]. Each stage of the chandelier decreases the temperature, first using liquid He cooling to get to 4 K, and then using dilution refrigeration to reach the mK range. The Joule heating of any interconnect reduces the efficiency of the refrigeration system, limiting how many qubits can be operated. Use of superconducting interconnects in a flexible ribbon would simplify the assembly and construct of interconnects, and a superconducting critical temperature above 4 K enables its operation in the liquid helium stages. Recently reported methods of patterning superconductors on flexible substrates include Ga-In-Sn and NbSe2 by inkjet [7, 8], Nb by sputtering and photolithography,[9] and YBCO on Kapton by an adhesive transfer method [10]. Aerosol jet printing (AJP) is an attractive method to pattern electronics devices because of its low cost compared with clean-room lithography techniques, < 10 µm resolution, and compatibility with a wide range of conductor and insulator materials [11]. Electrodeposition is a wet chemical process where material is deposited at the cathode and is widely used in the electronics fabrication industry. Methods to pattern electrodeposited material without the use of photolithography methods can be done by placement of masks over the cathode. Aerosol jet printing would enable the low-cost patterning of electrodeposited structures in a way that is easily modified, compatible with flexible substrates, and at < 10 µm resolution. Our group at Sandia has recently demonstrated the capability to pattern Cu and Ni by a combined AJP and electrodeposition process [14]. Re is a promising superconducting material because the amorphous form has a critical temperature of 5-6 K which makes it compatible with liquid He cooling. Huang *et al*. from the University of Alabama recently reported on a water-in-salt method to electrodeposit Re on Au substrates [15]. The water-in-salt method reduces the cracking of the films caused by hydrogen evolution and creates high quality films with a transition temperature of 5.8 K. The integration of an aerosol jet printed seed layer on flexible Kapton substrates with the water-in-salt electrodeposition process for deposition of Re should enable the patterning of flexible superconductors as a step towards fabrication of flexible superconducting ribbon cable interconnects for quantum computers.

Here, we propose an unprecedented approach to integrate aerosol jet printed silver (Ag) with rhenium (Re) electrodeposition for the advancement of superconducting interconnect

technologies. This combined approach would not only eliminate the aforementioned key roadblocks in scaling and the fidelity of quantum computing, but also offers the freedom of connection design, thus having the potential to dramatically change the landscape in which quantum computer currently resides and works.
For practical applications, materials that can be electroplated on flexible substrate and show superconductivity above the boiling point of liquid helium (4.2K) are desirable. Thin Re films have been produced by electrodeposition but only on rigid conductive substrates, such as metal, silicon, etc. Electrodeposition of amorphous Re has the potential to increase its superconducting critical temperature (Tc). The electrodeposition of Re onto a seed Ag trace deposited on Kapton using AJP is on the leading edge of research in this space. The combined processes, if successful, not only addresses the desired flexibility and weight of a superconducting cable but also increases the Tc of the material. In addition, AJP unlike any vacuum deposition process, offers ease of manufacturability, freedom of design and scalability to a continuous manufacturing process. Current interconnects with quantum chips are complex in their design and are subject to joule heating, temperature perturbations and thermal noise limiting processor fidelity/power/speed/scaling. The proposed technology seeks to reduce these limitations and simplify the design in the hope of strengthening our national security.

DETAILED DESCRIPTION OF RESEARCH AND DEVELOPMENT AND METHODOLOGY:

To explore and evaluate the integrated approach of aerosol jet deposition of a metal seed layer and the electrodeposition of rhenium we at SNL are collaborating with Professor Qiang Huang from the University of Alabama, Tuscaloosa, Alabama.

Sandia National Labs brings the direct write and aerosol printing expertise to this combined effort. The aerosol printer used in this research is the ‘Nanojet’, an ultrasonic aerosol jet printer from Integrated Deposition Solutions, Figure 1. The printer sits on a 3-axis motion-controlled gantry. Deposition of a range of materials including metals, dielectrics, magnetic and carbon nanotube-based inks is possible with this printer. In this work silver and gold inks are deposited as seed layers for electrochemically deposited rhenium. The Nanojet printer operates by generating an aerosol of a low viscosity fluid using an ultrasonic transducer. The aerosol is carried through the system by an aerosol gas and then focused by a sheath gas. In both cases house air is used. The aerosol mist passes through two focusing lenses, collimating the ink stream, and then deposited onto the desired substrate. The focusing lenses are a variable that one can select based on the requirements of the work. The first focusing lens, closest to the point where the ink mist exists the print head, is of larger ID than the second focusing lens, where the ink exists the print head, and range from 850 microns down to 100 microns. Linewidths as small as 12 microns can be printed with this system. Given this is a non-contact deposition process

with a standoff distance of 1-2 mm, conformal and stepped edge printing is possible. The substrate sits on a platen that moves in the x and y plane. The platen is typically heated to temperatures of 40-100°C depending on the material to set or 'pin' the part in place. Except in the case of reactive inks, all materials printed with the Nanojet must be cured or sintered to yield the desired properties. The metal inks used in this work, are sintered at 200°C for silver, 300°C for gold, for 3 hours to drive off organics, allowing particle coalescence which ultimately renders the materials conductive.

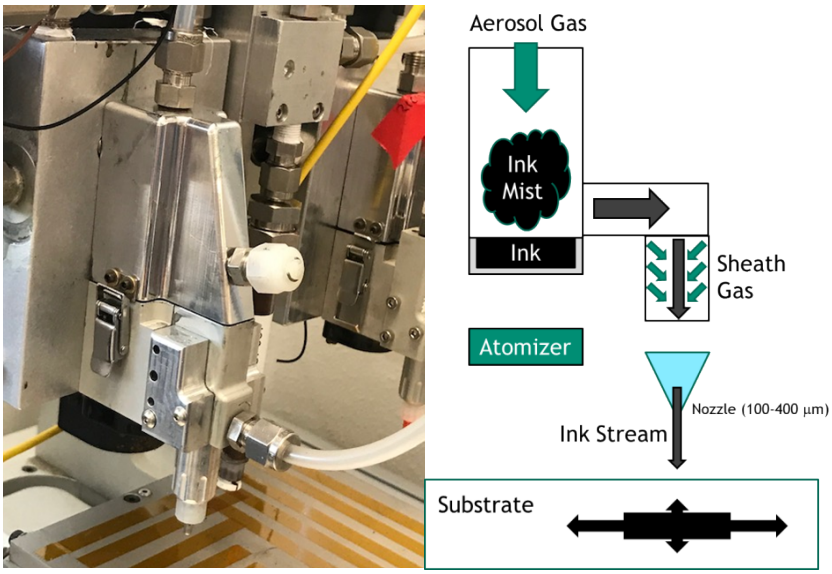

Figure 1. Picture (left) and schematic (right) of the 'Nanojet' aerosol jet printer.

UA (Prof. Huang's lab at University of Alabama) has developed a novel electrochemical deposition process to fabricate superconducting Re thin films on rigid silicon substrates. A conductive metal seed layer is typically deposited on Si with physical vapor deposition (PVD) methods and patterned into line shapes. The electrodeposited Re film therein is of amorphous nature and a superconducting transition temperature of around 6 K is reported, which is well above the He boiling point and thus makes the superconductivity much more accessible from the application point of view. UA brings this deposition technique to this joint effort to combine with AJP and enable the fabrication of such superconducting connecting lines on flexible substrates.

Kapton-metal seed layer substrates undergoing electrodeposition are mounted on a custom-made holder as the cathode, which rotates in electrolyte to provide solution agitation. As shown in Figure 2, a three-component electrochemical cell is used with a platinum anode, an Ag/AgCl reference electrode. An Autolab 302N potentiostat by Metrohm is used to provide the electrical current and voltage for electrodeposition. The Kapton substrate is fixed on the holder using plating tape and the electrical contact for electrodeposition is formed using a front contact pin. A

typical AJ printed metal (Ag or Au) pattern comprises a 1mm x 10 mm bar shape and a 2 mm x 2 mm pad. The bar pattern is used to deposit Re films for electrical and superconductivity characterization, and the pad is where the pin lands and forms the electrical connectivity. Therefore, the electrodeposited Re typically covers the entire metal pattern except for a circular footprint of the pin on the pad.

The Re electrodeposition is carried out using a so-called "water-in-salt" electrolyte, where a superhigh concentration of salt is present. More specifically, the electrolyte comprises 25 mM NH_4ReO_4 as the Re source, 0.1 M H_2SO_4 to ensure a highly acidic pH, and 5 M LiCl. The full hydration of this 5 M LiCl consumes a large amount of H_2O, thus depleting free water molecules, disrupting the hydrogen bond network in the electrolyte, limiting the hydrogen evolution reaction, facilitating the Re deposition and improving the film property.

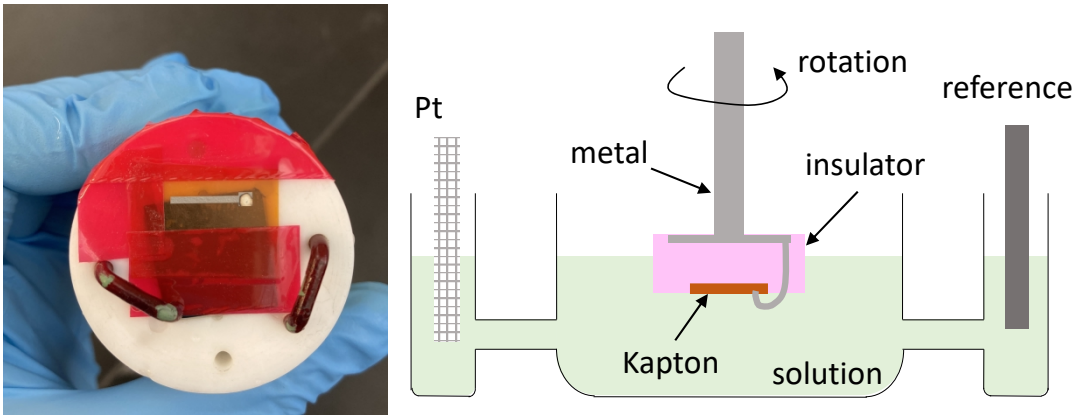

Figure 2. Picture (left) of the printed Au pattern on Kapton right after Re electrodeposition; and diagram (right) of the electrodeposition setup, where the Kapton film is mounted on a cathode holder in the electrolyte using a three-compartment electrochemical cell.

SNL has successfully demonstrated AJP deposition of metal-based inks that have served as a seed layer in the electrodeposition of copper. UA has successfully carried out the electrodeposition of Re on vacuum deposited Au and other metal films on rigid substrates and has demonstrated the superconductivity of Re with an enhanced critical temperature above 4.2 K. Here research was conducted to understand the viability and identify the challenges of integrating both AJP and Re electrodeposition processes on flexible substrates.
The highly flexible, stable and temperature resistant polyimide substrate, Kapton, was used in this research. Different gauges of Kapton were selected and treated by varying means so to identify the best candidate substrate. Silver was chosen as the preferred seed metal given its high conductivity, ability to successfully print with AJP and significantly, its lower cost. This would serve as the first attempt to electrodeposit rhenium on silver. Gold was identified as a second, alternate seed material primarily due to cost. SNL has much experience in printing of gold. UA

has successfully demonstrated rhenium electrodeposition on gold. Following rhenium electrodeposition, structural, mechanical, and electrical characterization of the composite was conducted.

METHODS:

Solution based UTDots Ag40X, and UTDots Au40X were used for this work. The as received inks were re-formulated to optimize the printed ink resolution as identified in previous work. Silver ink formula - Ag40X 20 vol%, Terpineol 20 vol%, xylenes 60 vol%; Gold ink formula - Au40X 40 vol%, Terpineol 20 vol%, xylenes 40 vol%. All printing was carried out with a travel speed of 300 mm/min, 4-layer depositions and with a platen temperature of 100°C. A Lennox Laser 750 µm orifice first focusing lens and a Fisnar 160 µm Micron-S Precision tip second focusing tip were used to collimate the ink stream for all prints. Print head deposition conditions were optimized for each material. Silver optimized deposition conditions: atomizer voltage- 18V, aerosol gas- 4.0 SCCM, sheath gas- 40 SCCM. The sheath gas is passed through a glass jar containing xylenes to prevent the aerosolized ink from drying out. Gold optimized deposition conditions: atomizer voltage- 20V, aerosol gas- 4.0 SCCM, sheath gas- 40 SCCM again passed through a glass jar containing xylenes. Printed inks were sintered in an oven under atmospheric conditions at 120°C for 3 hours for silver and 300°C for 3 hours for gold. Kapton film purchased from Granger was used for all but the last set of experiments presented in this report. Granger Kapton was backordered to the end of the year. Thus, for the last set of experiments Kapton was purchased from Global Industrial however material differences from vendor to vendor can be significant. ASTM 3359 Tape test was followed to determine the extent adhesion printed and electrodeposited materials to Kapton. A razor blade was used to section each 1x1 cm square into 6x6 smaller squares. Samples were cleaned gently with nitrogen to remove debris created by the razor blade. ASTM 3359 Tape was applied to each sample and smoothed so that it made uniform contact. The tape was peeled in a 180-degree direction to AJP depositions. Optical micrographs were acquired on Keyence VH-Z100R and VH-Z00R optical microscopes. Adhesion tests of the printed seed metal and the seed metal-rhenium composite on Kapton were carried out according to the ASTM D3359 Tape Test. The classification of adhesion test results chart is shown in Figure 3.

CLASSIFICATION OF ADHESION TEST RESULTS

CLASSIFICATION	PERCENT AREA REMOVED	SURFACE OF CROSS-CUT AREA FROM WHICH FLAKING HAS OCCURRED FOR SIX PARALLEL CUTS AND ADHESION RANGE BY PERCENT
5B	0% None	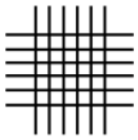
4B	Less than 5%	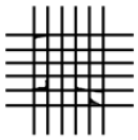
3B	5 – 15%	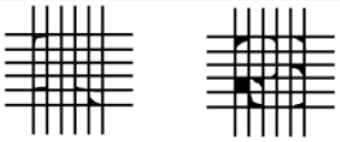
2B	15 – 35%	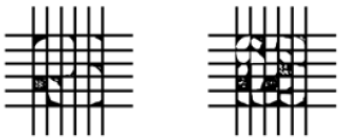
1B	35 – 65%	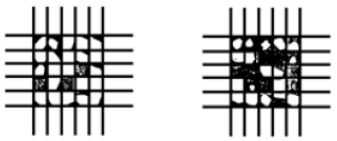
0B	Greater than 65%	

Figure 3. Table of ASTM D3359 tape test classification of adhesion test results.

To ensure maximum adhesion of the AJP seed metal to the Kapton substrate, two thicknesses of Kapton – 127 micron and 500 microns - were initially explored. The 500-micron thick Kapton being significantly thicker, is more rigid compared to the 127-micron film. Kapton films were evaluated in two forms – as received and roughened with sandpaper. Several grits of sandpaper were evaluated initially to determine the preferred level of coarseness – 320, 600 and 1200 (smoothest). Kapton film was roughened by hand in a random direction. All Kapton films, both as received and roughened were cleaned by sonicating in isopropyl alcohol for 15 minutes, prior to AJD of seed metals. Bend tests were carried out on samples approximately 4mm wide, 15mm long with a thickness ranging from 0.140-0.167mm. 3-point bend tests were conducted in an RSA G2 (TA Instruments) with a 10mm support span fixture. The samples were tested first with the printed silver/gold side face up, then retested with the printed side face down. Samples were

tested at a strain rate of 0.1mm/mm/min as recommended in ASTM D790, while the axial load was recorded. On passing through the yield point tests were stopped. The yield point is seen on a stress-strain curve as the maximum stress and corresponding strain. It is the stress and strain at which a material transitions from elastic deformation to plastic deformation. During elastic deformation, a material will return to its original shape once the applied load has been removed. Once plastic deformation begins, the material will be permanently deformed. Upon completion of 3-point bend testing, the samples were reused for cyclic bend testing in a 3-point bend orientation. The RSA G2 with a 10mm support span was again used for the test. Samples were tested with the printed silver/gold side face down. A strain of 1.27% was applied at a frequency of 0.033Hz and 0.032Hz for the smooth and roughened samples respectively. This frequency corresponds with a strain rate of 0.1mm/mm/min, matching the strain rate of the 3-point bend tests. The test ran for 200 cycles and measured the axial load during bending. The thickness of electrodeposited Re is determined using a Bruker M1 Mistral X-ray fluorescence spectroscope (XRF) with a 0.7 mm collimator and 50 kV excitation voltage. The morphology of electrodeposited Re films is characterized using a Thermal Scientific™ Apero field emission scanning electron microscope (FE-SEM) equiped with a Bruker Energy Discpersive X-ray Spectrometer (EDS). The later is used to acquire the elemental mapping to characterize the uniformity or coverage of the deposited Re. It is also used to characterize the cross-section of the film stack on Kapton. In this later case, a FEI quanta focus ion beam (FIB) station is used to cross section and polish the film stack. Crystallographic characterization of the films is carried out using a Bruker D8 diffractometer. Electrical resistance of the AJ printed seed layer and the fully deposited film stack are determined using a 4-point probe setup on the bar pattern with a current source and microvoltameter. The superconducting critical temperature or transition temperature of the electrodeposited Re films is measured using a Quantum Design Dynacool Physical Property Measurement System (PPMS). This transition is determined by recording the film resistance along with temperature sweep from 30 K down to 1.8 K. A four-probe configuration is used for the resistance measurement. Dupont 4929N™ silver paint is used to form four connections between the deposited film and the resistivity puck. Thermogravimetric Analysis (TGA) was performed on reformulated UTDots Ag40X and UTDots Au40X using a Netzsch STA 490C/CH for Ag40X and a TA Instruments SDT 2960 for Au40X. Both inks were characterized in an air atmosphere at a ramp rate of 1°C/min. The data from room temperature to 500°C is plotted in Figure 4. The most volatile solvent is Xylenes (vapor pressure at 100°C = 0.36 bar), followed by terpineol (vapor pressure at 100°C = 0.017 bar). We assign the first shoulder to xylenes evaporation followed by terpineol at 125°C. A gradual decrease in mass for both Ag and Au at temperatures above 125°C may result from surfactant burn-off.

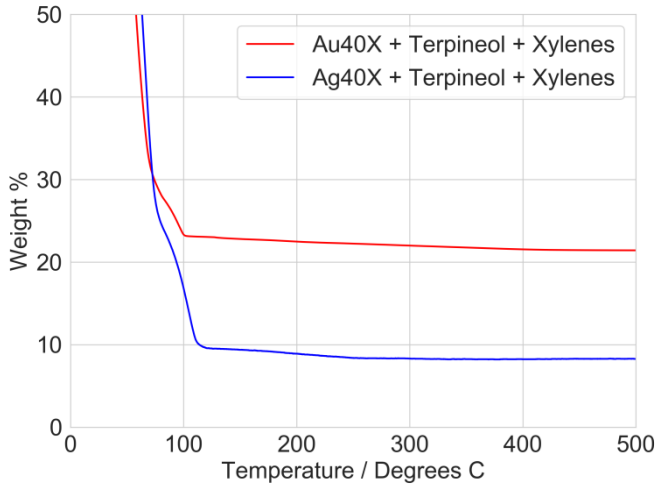

Figure 4. TGA of re-formulated UTDots Ag40X and UTDots Au40X in air atmosphere.

RESULTS AND DISCUSSION:

Adhesion Studies

Reformulated UTDots Ag40X with terpineol and xylenes was deposited on the as received and roughened Kapton with a platen temperature of 100°C, sintered and then tested for its adhesion according to the ASTM Tape Test. The results on 500-micron thick Kapton are shown in Figure 5. As received, smooth Kapton resulted in complete loss of printed silver upon removal of the tape and a rating of 0B. The 320 grit experienced some loss of material and received at rating of 3B. The Kapton roughened with 600 grit sandpaper showed no loss of material. The tape was applied twice here and maintained no loss and a rating of 5B. 1200 grit roughened Kapton experienced almost complete loss of material and received an ASTM rating of 0B. Overall, initial results on 500-micron thick Kapton indicated this material was too rigid for the intent of this work. Stresses were readily building in AJP silver ink that were attributed to the rigidity of the substrate. In addition, preliminary results from electrodeposited rhenium on 500-micron thick Kapton roughened with 600 and 320 grit sandpaper showed the deep scouring caused by the coarse paper presented some issues to rhenium electrodeposition. While the very coarse roughening yielded excellent results from an adhesion perspective based on these results it was decided 127-mircon thick Kapton in the smooth as received form and roughened with 1200 grit sandpaper would be the substrates of focus.

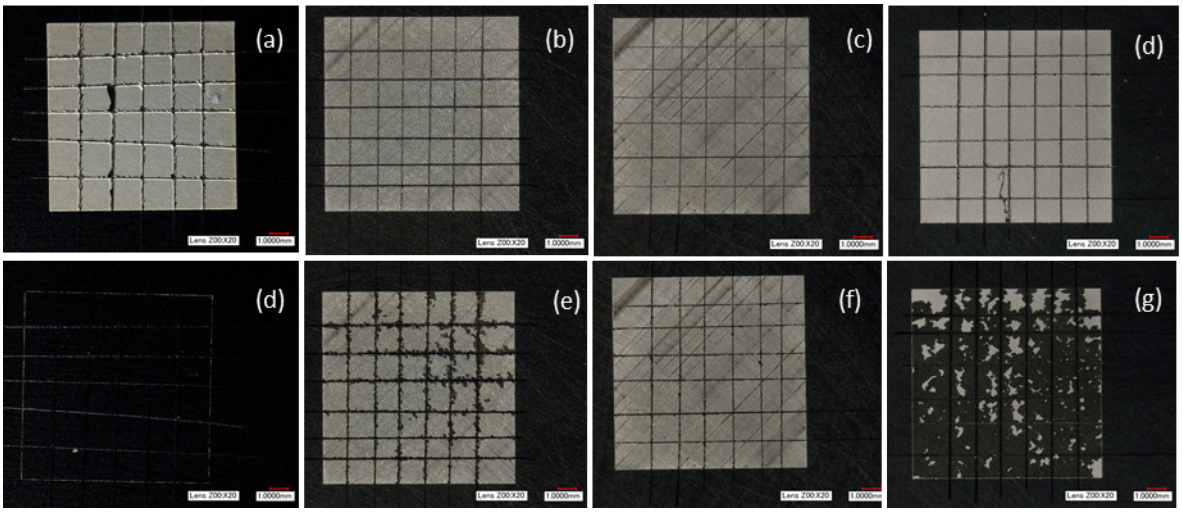

Figure 5. Microscopy images of AJP Ag on 500-micron Kapton. Before (a-d) and after (e-h) ASTM adhesion tape test. Images are on smooth Kapton (a & e), Kapton roughened with 320 grit sandpaper (b & f), Kapton roughened with 600 grit sandpaper (c & g) and Kapton roughened with 1200 grit sandpaper (d & g).

Silver prints were deposited on 127-micon Kapton. Figure 6 shows tape test results for smooth, unroughened Kapton and Kapton roughened with 1200 grit sandpaper. The results on the thinner more flexible substrate were significantly different to that on 500-mircon think Kapton. As received, smooth Kapton experienced minimal loss and received a rating of 4B. Kapton roughened with 1200 grit sandpaper showed no loss of material and received a 5B rating.

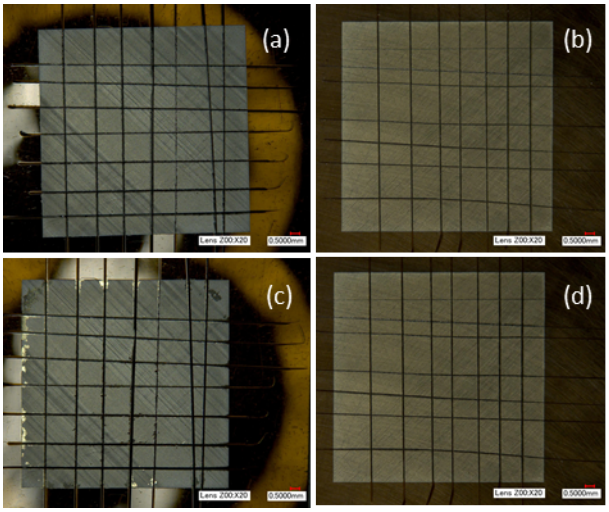

Figure 6. Microscopy images of AJP Ag on 127-micron Kapton. Before (a & b) and after (c & d) ASTM adhesion tape test results. Images on smooth Kapton (a & c) show a 4B rating (<5% loss) and on Kapton roughened with 1200 grit sandpaper (b & d) show a 5B rating (0% loss).

We were interested to see if a higher sintering temperature of 300°C versus 120°C would improve the extent of adhesion of silver on Kapton. Silver ink was deposited on smooth and 1200 grit roughened Kapton. One sample was sintered at 120°C/3 hours; the other at 300°C/3 hours. Figure 7 (a & b) shows the results show the results of silver deposited on smooth Kapton. Figure (a) was sintered at 120°C for 3 hours. This material showed some loss (5-15%) and received a 3B rating. Figure 7 (b) was sintered at 300°C for 3 hours also showed some loss (5-15%) and received a 3B rating. Figures (c & d) printed on Kapton roughened with 1200 grit sandpaper showed quite different results depending on sinter temperature. Figure (c) sintered at 120°C for 3 hours showed no loss and received a 5B rating. Figure (d) shows that the higher sinter temperature of 300°C significant loss (35-65%) occurred and received a rating of 1B. Thus, the adhesion of silver to roughened Kapton is superior to smooth Kapton but the extent of the adhesion is dependent on sintering temperature. A sintering temperature of 120°C for Ag shows stronger adhesion than that at 300°C. Further investigations are needed to understand the surface interactions at the different temperatures.

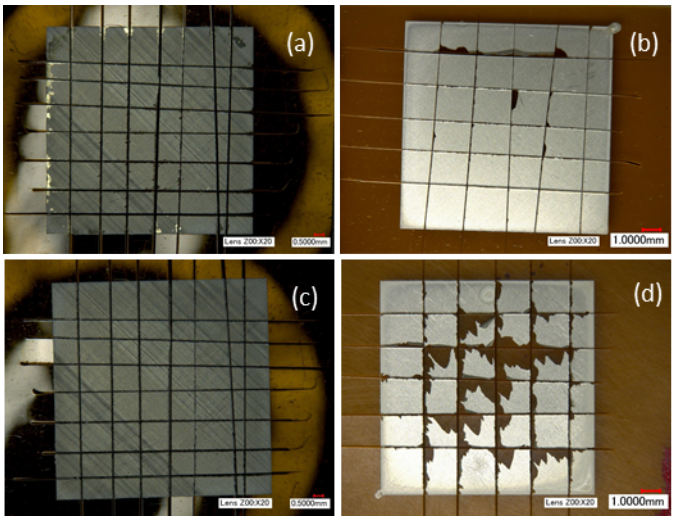

Figure 7. Microscopy images post ASTM adhesion tape test of AJP Ag on smooth (a & b) and 1200 grit roughened (c & d) Kapton. Figures (a & c) were sintered at 120 C for 3 hours. Figures (b & d) were sintered at 300 C for 3 hours. Figure (a) received a 3B rating (5-15% loss). Figure (b) received a 3B rating (5-15% loss). micron Kapton. Figure (c) received a 5B rating (0% loss). Figure (d) received a 1B rating (35-65% loss).

In addition to AJP silver as the seed layer for rhenium electrodeposition, AJP gold was also evaluated. Results of AJP Ag on thick Kapton, both smooth and roughened with sandpaper, were

found to be suboptimal and thus not evaluated with AJP gold. Reformulated UTDots Au40X was deposited on smooth and 1200 grit roughened, 127-micron Kapton. Samples were sintered at 300°C for 3 hours. Adhesion tape test results are shown in Figure 8. Smooth, as received Kapton shows minimal loss (<5%) of gold upon removal of the tape, with a 4B rating. Figures (b & d) show before and after images of Kapton roughened with 1200 grit sandpaper. Here, no loss (0%) of gold occurred for either substrate post tape test and received a rating of 5B.

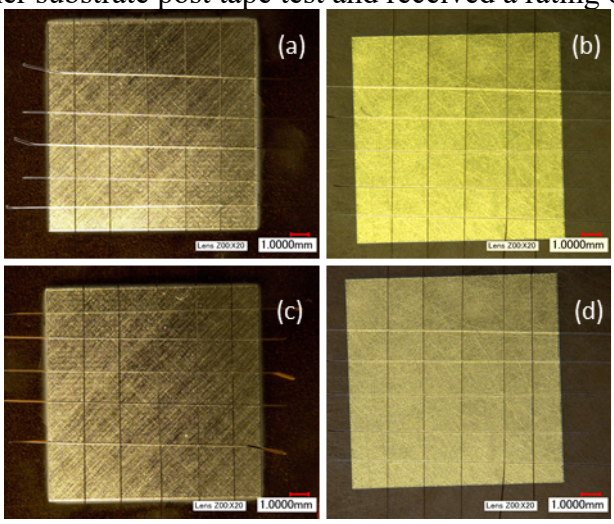

Figure 8. Microscopy images of AJP Au on 127-micron Kapton. Before (a & b) and after (c & d) ASTM adhesion tape test results. Before and after images on smooth Kapton (a & c) show a 4B rating (<5% loss). Before and after images of Kapton roughened with 1200 grit sandpaper (b & d) show a 5B rating (0% loss).

Adhesion tests on rhenium electrodeposited on gold on Kapton are shown in Figure 9 (details in following section). Efforts to evaluate the adhesion of rhenium on silver were not possible due to complete delamination of the composite as shown in Figure 10. Electrodeposited rhenium on smooth and roughened Kapton are shown in Figures (a & d) prior to sectioning. Figures (b & e) show images of the samples prior to tape test and Figures (c & f) post tape test. Smooth, as received Kapton showed some loss (15-20%) of composite upon removal of the tape, with a 2B rating. Kapton roughened with 1200 grit sandpaper showed minimal loss (<5%) with a 4B rating. We viewed these results as very successful, especially in the case of Kapton roughened with 1200 grit sandpaper.

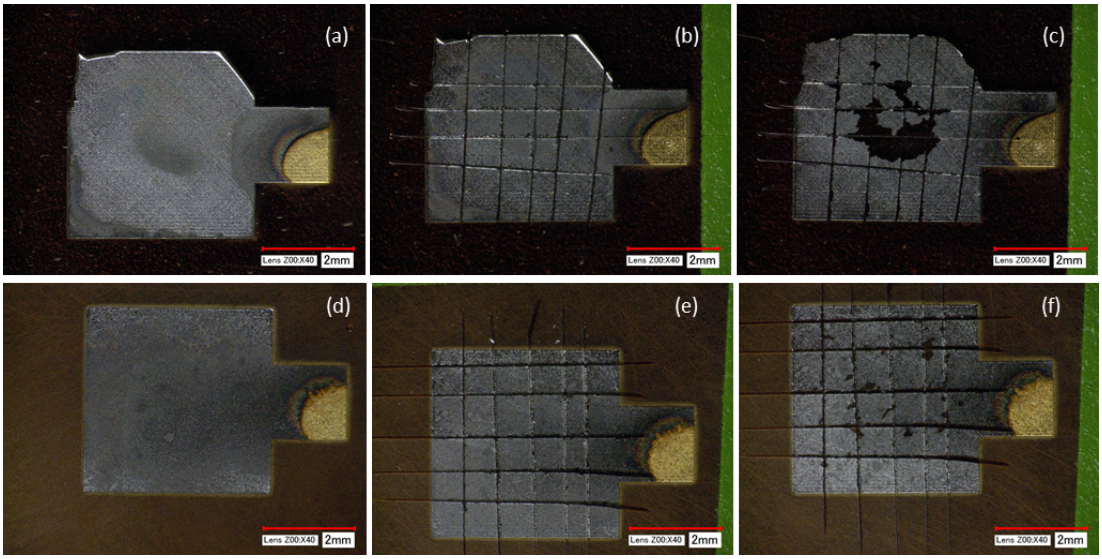

Figure 9. Microscopy images of electrodeposited Re on AJP Au on smooth (top row) and roughened (bottom row) 127-micron Kapton. Prior to sectioning (a & d), before (b & d) and after (c & f) ASTM adhesion tape test. Images on smooth Kapton (c) show a 2B rating (15-20% loss) and roughened Kapton (f) a 4B rating (<5% loss).

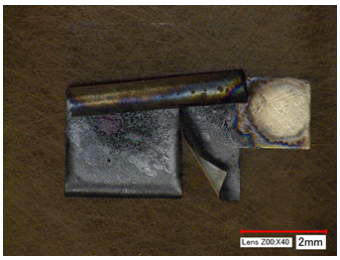

Figure 10. Microscopy images of AJP Re on Ag on 127-micron Kapton roughened Kapton. Complete delamination occurred.

Electrodeposition

Four types of substrates were transferred to UA for the electroplating studies. As shown in Figure 11, AJP Ag and Au ink was deposited on smooth Kapton and Kapton films roughened with sandpaper. The thickness of AJ printed layer was measured using a stylus profilometer. A thickness of 3.260 ±0.262 µm on roughened and 4.053 ±0.281 µm on smooth Kapton for Ag and 1.618 ±0.462 µm on roughened and 0.854 ±0.142 µm on smooth Kapton for Au were measured respectively. The sheet resistance of the layers was measured using a 4-probe setup on the 1mm x 10mm bar pattern. Resistances between 0.2 to 0.3 ohm for Ag and between 1.5 to 1.6 ohm for Au were measured.

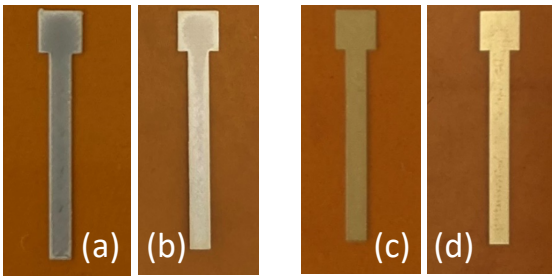

Figure 11. AJ printed (a, b) Ag and (c, d) Au on 127 um thick (a, c) smooth Kapton and (b,d) Kapton films roughened with 1200 grit sandpaper.

Initially, Re electrodeposition study is carried out to deposit about 450 nm Re on Ag layer printed on smooth 127 µm Kapton films. Delamination was observed for all the plating current densities used and all the Re film thickness studied. The same study was repeated using Ag printed on Kapton films roughened with sandpaper of different grits, however, resulting in the same delamination, shown in Figure 12 (a,b).

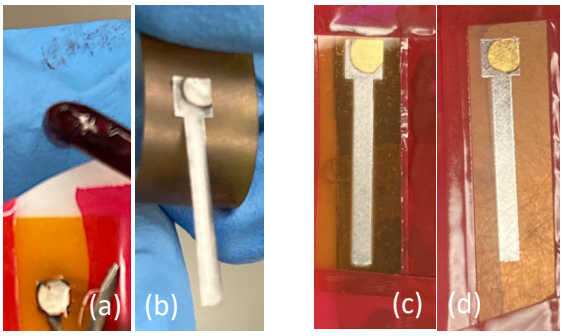

Figure 12. Electrodeposition of about 400 nm Re on (a,b) Ag, and (c,d) Au layers AJ printed on (a,c) smooth and (b,d) roughened Kapton.

Because the Re electrolyte used in this study is highly acidic, a study is conducted later to determine if the dissolution of Ag layer in this acidic solution occurs and, if so, if it is responsible for the delamination. It is found that the Ag layer does dissolve in this electrolyte after being immersed for 24 hours. However, the Re deposition takes only 10 minutes and the Ag is under negative bias during deposition, which is expected to significantly slow down the anodic dissolution of metal. Therefore, the dissolution of Ag is believed not to be responsible for the delamination. To further confirm this, a different Re electrolyte with a pH 6 containing 25 mM NH_4ReO_4 and 5.2 M NH_4CH_3COO is used to deposit Re on Ag. In this study, the same delamination is observed whilst the Ag does not dissolve at all at this high pH of 6. The internal stress of electrodeposited Re is believed to act in conjunction with an insufficient adhesion between Ag and Kapton to cause this delamination. Pulsed current schemes (instead of DC currents)

and thinner Re films are attempted to lower the film stress, but with little to no success in avoiding the delamination.

On the other hand, AJ printed Au layer on the same Kapton films are also used for the study. Initially, it is chosen as an alternative metal with much better corrosion resistance. While later studies find that the delamination of Re on Ag is not due to the dissolution as the discussed above, Re films deposited on AJ printed Au are found adherent to the substrate. As shown in Figure 12 (c) and (d), the films are entirely attached to the Kapton after electrodeposition for both types of Kapton substrate. This much improved adherence sustains even when the Re film thickness increases for over 5 times from under 500 nm to over 2.6 um.

While the AJ printing of Au and Ag use identical solvents, they require different curing processes: 120°C for Ag and 300°C for Au. Additional studies are carried out, where the printed Ag is cured at 300°C, to dissect the effect of curing temperature. Yet, the electrodeposited Re delaminates on Ag cured at this high temperature, suggesting some intrinsic difference in the printed Ag and Au.

Another study carried out with Ag investigates Kapton roughened with different grit (600 to 1200) sandpapers. It was found that the lower grit (600 and 800) sandpaper appears to improve the adhesion after Re electrodeposition. However, such improvement is marginal and partial delamination still takes place.

Cross sectional characterization of the full film stacks

Because the metal layer delaminates from the Kapton substrate upon Re electrodeposition and prevents further characterization, a sample with only printed Ag layer (before Re deposition) is used for cross sectional characterization. The film is sectioned and polished using FIB and characterized using an FE-SEM. Figure 13 shows the images of an inner cross sectional cut within the Ag pattern. The Kapton substrate is roughened with 1200 grit sandpaper, which appears to create the roughness observed in the SEM images. The AJ printed Ag shows a columnar grain structure. In addition, a clear adherent interface is observed between Ag and Kapton with no delamination. However, another cross section is prepared by cleaving the film and polishing the edge surface. Figure 14 shows the SEM image, where the film detachment already takes place during the sample handling and sectioning. An EDS line scan is also performed across the cross-section and confirms this crevice, where the Ag signal sharply decreases.

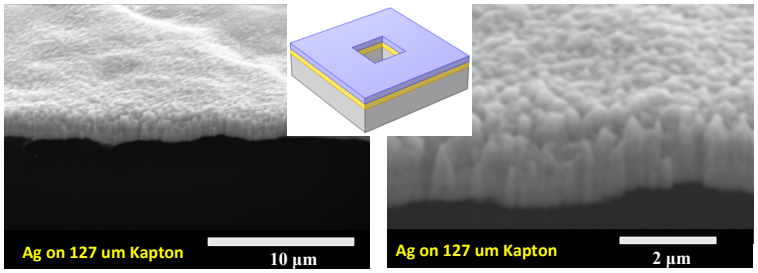

Figure 13. SEM image of a cross section in AJ printed Ag layer on Kapton. The diagram at center shows the inner cross sectioning.

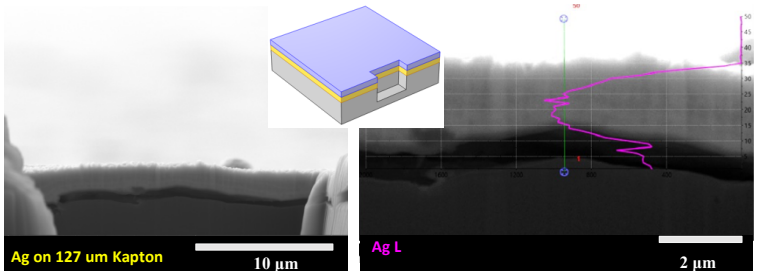

Figure 14. SEM image and EDS line scan across the edge cross section (shown in diagram) of AJ printed Ag layer on Kapton.

To compare with Ag, similar analysis is performed for Au patterns. Shown in Figure 15 is a cleaved and polished edge cross section of Au pattern after Re electrodeposition. This is the most challenged case. Not only does the deposited Re layer introduce stress and tend to delaminate the film but also the cross sectioning is performed at a cleaved edge (illustrated by the diagram in Figure 14). However, an almost perfectly adherent interface is observed between the metal and Kapton. In addition, the Re and Au interface is also clearly observed with no apparent intermixing, consistent with expectation. Columnar grain structure is also evident for AJ printed Au. This result is confirmed with another cross sectioning inside the pattern (illustrated by the diagram in Figure 13) and similar perfect interface is observed.

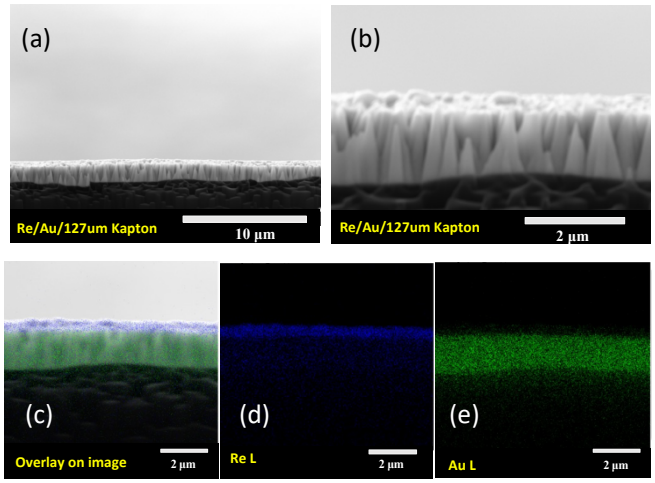

Figure 15. (a,b) SEM images and (c,d,e) EDS elemental mapping of an inner cross section of electrodeposited Re on AJ printed Au layer on Kapton.

This cross-sectional characterization of the film stack clearly confirms the visual observation of the different adhesion between Ag and Au. It is interesting that the two metals printed using similar chemistry and process result in such drastically different results. Some efforts have been devoted to dive deep to find out the mechanism for this. For example, as mentioned earlier, printed Ag layers annealed at 300°C (instead of 120°C) didn't improve the adhesion. Preliminary thermal gravimetric analysis microgravity analysis shown in Figure 4 was carried out to characterize the mass loss during curing due to solvent evaporation, but no clear difference or conclusion can be drawn yet.

Film resistance measurements

Film resistance is measured using a 4-probe setup on the 1 mm x 10 mm bar pattern. A small constant current (about 10 mA) is applied through the two end leads on a set of AJ printed layers on 1200 grit roughened Kapton and smooth Kapton. Simultaneously, the voltage between the two central leads on the film is recorded using a micro-voltameter. The results are presented in the following tables.

Table 1: Resistance of AJP Au on 127 um 1200 grit polished Kapton.

Substrate No	Applied Current (mA)	Voltage (mV)	Resistance (V/I) (Ω)
01	9.99	1.69	0.169
02	9.99	1.83	0.183
03	9.99	1.76	0.176
04	9.99	1.79	0.179

Table 2: Resistance of AJP Au on 127 um smooth Kapton.

Substrate No	Applied Current (mA)	Voltage (mV)	Resistance (V/I) (Ω)
05	9.98	1.56	0.156
06	9.98	1.58	0.158
07	9.98	1.48	0.148
08	9.98	1.49	0.149

Table 3: Resistance of AJP Ag on 127 um 1200 grit polished Kapton.

Substrate No	Applied Current (mA)	Voltage (mV)	Resistance (V/I) (Ω)
09	9.98	0.29	0.029
10	9.98	0.26	0.026
11	9.98	0.30	0.030
12	9.98	0.28	0.028

Table 4: Resistance of AJP Ag on 127 um smooth Kapton.

Substrate No	Applied Current (mA)	Voltage (mV)	Resistance (V/I) (Ω)
13	9.97	0.25	0.025
14	9.97	0.26	0.026
15	9.97	0.27	0.027
16	9.97	0.25	0.025

It is evident from the above tables that the resistance of AJ printed metal films does not vary significantly for a same type of metal. It was reported in literature that the surface roughness can sometimes affect the sheet resistance for printed conductive films [16]. Here, the metal films printed using AJ apparently have a reproducible and smooth surface, resulting in minimum variation in the resistance measurements.

The distance between the 4 probes is fixed at 2 mm. Therefore, the distance between the two current leads is 6 mm, much larger than the width of the bar pattern, 1 mm. A quick numerical simulation confirms that the current flows in parallel with the pattern and the measured resistance can be described by the equation below, where is ρ is the resistivity, L is the length of the conductor or the distance between the voltage leads, 2 mm in this case, W is the width of the conductor, 1 mm in this case, t is the thickness of conductor, and R_s is the sheet resistance, defined as the ratio between resistivity over thickness.

$$R_{measure} = \rho \cdot \frac{L}{W \cdot t} = \frac{\rho}{t} \cdot \frac{L}{W} = R_s \cdot \frac{L}{W} = 2\,R_s$$

The measured resistance for printed Au layers ranges from 0.15 to 0.18 ohm. This corresponds to a sheet resistance between 0.075 and 0.09 ohm/sq. Considering the film thickness measured with profilometry for Au layer from 0.85 to 1.6 um, this suggests a resistivity of AJ printed Au from 6.4E-8 to 14.4E8 ohm-m, about 3 to 6.5 times higher than the intrinsic resistivity of Au metal (2.2E-8 ohm-m). On the other hand, the printed Ag layers have the measured resistance at 0.025 to 0.030 ohm and thickness at 3.2 to 4.0 um. The corresponding resistivity is 4E-8 to 6E-8 ohm-m, or 2.5 to 4 times higher than the bulk Ag metal. This is consistent with literature reports [17,18].

The film resistance is also characterized after Re electrodeposition on each type of the substrates. The Re electrodeposition is carried out using the same process under same condition, resulting in a reproducible thickness between 400 to 500 nm. The small variation is expected from experimental electrodeposition process and the XRF measurement. As shown in Table 5, the resistance of the film stack slightly decreases after Re deposition due to the additional conductive path in Re. But the overall resistance of the film is apparently dominated by the AJ printed seed layer (Au or Ag). The effect of the Re layer on top can theoretically be viewed as a conductive path in parallel with the seed. But a quantitative calculation of this effect is not practical because the resistance variation of the seed layer itself overwhelms the effect of Re layer.

Table 5: Resistance of ECD Re on AJP metals on 127 um smooth and 1200 grit polished Kapton.

Substrate	Re Thickness from XRF (nm)	Resistance (Ω) Before Re Deposition	Resistance (Ω) After Re Deposition
Au on 1200 grit Polished Kapton	496	0.169	0.164
Au on smooth Kapton	466	0.158	0.154
Ag on 1200 grit Polished Kapton	420	0.029	0.025
Ag on smooth Kapton	466	0.025	0.020

Crystallographic structure, Morphology, Composition, and Superconductivity of ECD Re

It is known from UA team's previous studies that Re films electrodeposited on rigid substrates (Si) has an amorphous structure [19,15]. Figure 16(a) shows the X-ray diffraction (XRD) patterns of ECD Re on Ag AJ printed on the Kapton roughened with 1200 grit sandpaper. Two Re films are presented here, both deposited under the same conditions and at the same potential of -1 V. The deposition times are different resulting in two different thickness, 81 and 241 nm. The intensity on y-axis is in log scale to ease the comparison. The only strong sharp peaks observed for both

samples are from Ag. Broad background peaks at 2θ values between 40º to 55º are observed for both samples, corresponding to the amorphous structure of as deposited Re.

Figure 16(b) shows the topdown SEM characterization of the same Re films, where a nodular surface is observed for thin film and sporadic pyramid shaped crystals are observed for thick films. UA team's previous studies showed that electrodeposited Re film can be smooth on polished bulk metal substrates [19]. On the other hand, when Re is co-deposited with another element to form alloy films, such as ReCo and ReFe, the film morphology can become nodular depending on the potential used [20,21]. Here, it is believed that the film morphology of electrodeposited Re is strongly influenced by the AJ printed seed layer. This is not only because of the morphology of seed layer itself but also because the Re nucleation and growth behavior on printed seed can be completely different from on bulk metal or PVD seed on Si.

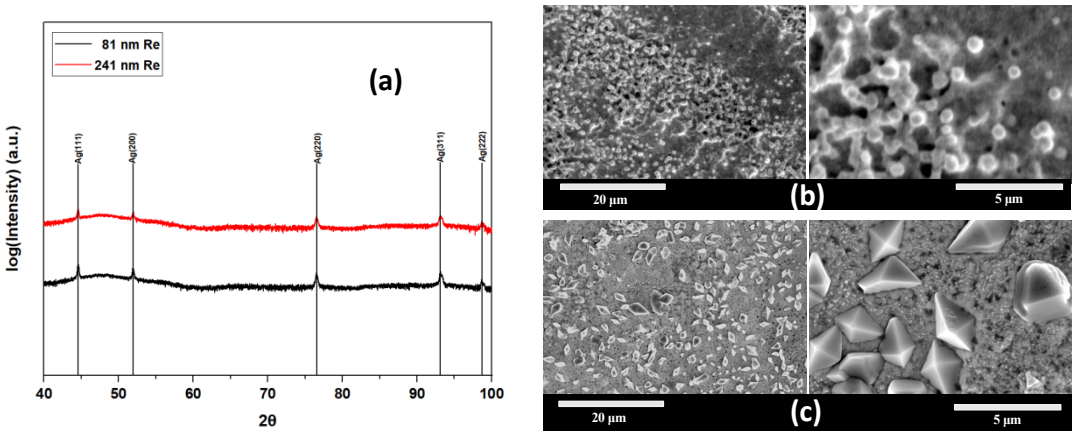

Figure 16. (a) XRD and topdown SEM images of (b) 81 nm and (c) 241 nm Re films electrodeposited on Ag printed on the Kapton roughened with 1200 grit sandpaper.

To further characterize the ECD Re, topdown elemental map is acquired for the same two films using SEM-EDS and the results are shown in Figure 17. No brightness / contrast adjustment was performed and the scale bar of the signal intensity is included in the images to allow for a rough comparison between the two images.

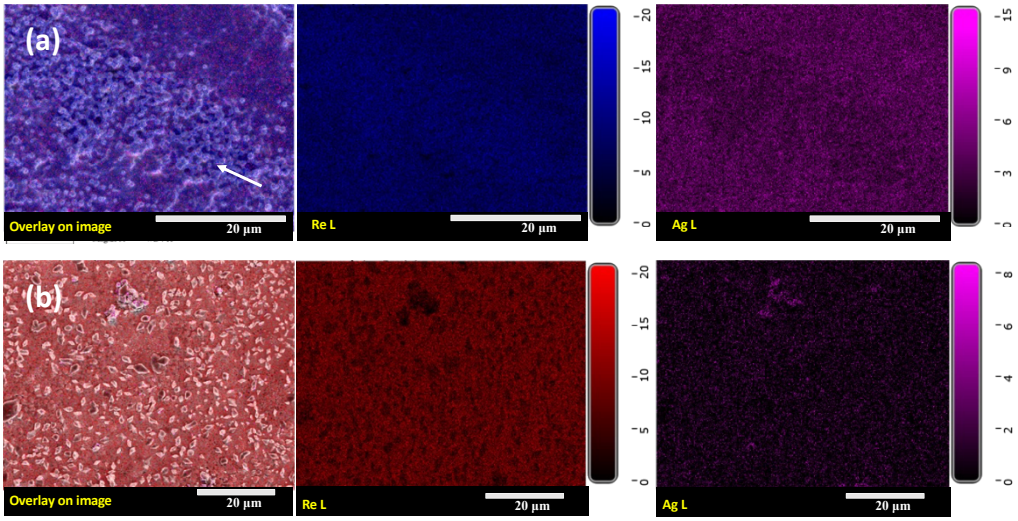

Figure 17. Topdown EDS elemental map for (a) 81 nm and (b) 241 nm Re films electrodeposited on Ag printed on the Kapton roughened with 1200 grit sandpaper.

For the 81 nm Re sample, significant Ag signal was observed across the surface. The Re coverage is relatively uniform. However, there are slightly higher Re and lower Ag signals for the region along the diagonal of the image, indicated with the white arrow, where more nodular features are observed on SEM. This suggests that the nucleation and growth of very thin Re can be challenging and the film may or may not be completely coalescent on AJ Ag seed. On the other hand, a uniform coverage of Re with strong Re signal is observed for the 241 nm Re sample. The Ag signal from the seed is much suppressed, with a much darker Ag map despite of a magnified color scale of Ag signal. Furthermore, the pyramid shaped crystals on the surface correspond to lower Re signal but not higher Ag signal. This suggests that the crystals are of a lower Re content, less than 100% pure Re. Further analysis using higher magnification tools such as TEM would be needed in future to determine the speciation and to determine whether such crystals form during electrodeposition or due to any post deposition reaction.

The two Re films were also characterized in a Quantum Design Dynacool Physical Property Measurement System (PPMS) for the superconducting behavior. The film resistance is measured with a 4-point probe configuration as temperature is swept from 30 K to 1.8 K. Figure 18 shows the resistance transients. For the 241 nm Re, a relatively sharp transition was observed, where the resistance quickly drops at 5.9 K, then almost to 0 ohm at 5.6 K. However, the resistance drop slows down and does not reach 0 ohm until 5.2 K. Bulk crystalline Re has a transition temperature, or critical temperature (Tc), of 1.8 K. This much improved Tc of 5.2 K is known due to the amorphous structure for electrodeposited Re. This Tc is above the boiling point of liquid helium and is considered as a first successful demonstration of such improved Tc on AJP metal seed.

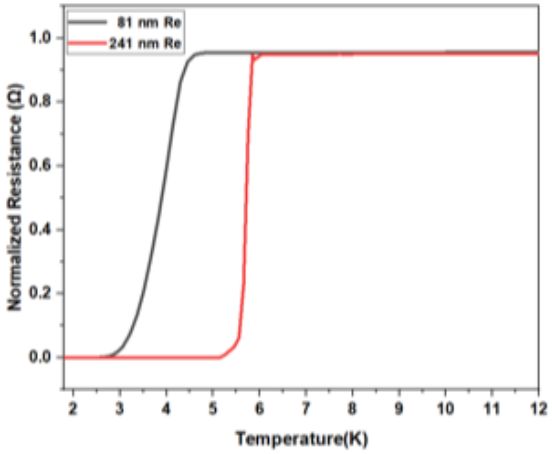

Figure 18. Superconducting transition of (a) 81 nm and (b) 241 nm Re films electrodeposited on Ag printed on the Kapton roughened with 1200 grit sandpaper.

The much thinner 81 nm Re film shows a much more sluggish transition and a much lower Tc. The resistance drop starts at 4.6 K and reaches 0 ohm at 2.8 K. A previous study by UA [15] on rigid Si substrate showed a dependency of Tc on the film thickness, where such transition becomes more difficult (lower Tc) when the films become significantly thinner. For example, a Tc of 3.1 K was reported for a 90 nm Re film, similar to the 81 nm case here. However, the transition for the 90 nm film on Si occurs between 4.1 K to 3.1 K, much sharper than the 81 nm case here. This might be related to a more pronounced thickness variation in the Re film deposited on printed Ag. While such variation may be present regardless of the film thickness, the Tc is expected to be more sensitive to this variation when the overall thickness is small.

It is worth noting that Re electrodeposition on AJP Ag seed results in the delamination between metal from Kapton. The above characterization was performed after carefully taping down the delaminated film on a Kapton substrate. It only serves as the film property characterization and does not mean such films can be of practical use. Some efforts are put into attempts to improve the adhesion before AJP Au becomes the main focus. For example, pulse electrodeposition is carried out, where the scheme comprises a deposition step at -1 V for 30 seconds and a pause at open circuit for 30 seconds. The cathode holder rotates at 400 rpm during the deposition step and the rotation stops during the pause. This cycle is repeated 10 times, equivalent to a DC deposition of 300 seconds. Unfortunately, while such pulse deposition scheme often lowered the film stress, partial but significant delamination is still observed. The parts retained on Kapton are used for some characterization and Figure 19 shows the XRD pattens and resistance drop for two of the pulse deposited films. Both films showed amorphous grain structure and similar transition with an elevated Tc at 4.9 and 5.3 K.

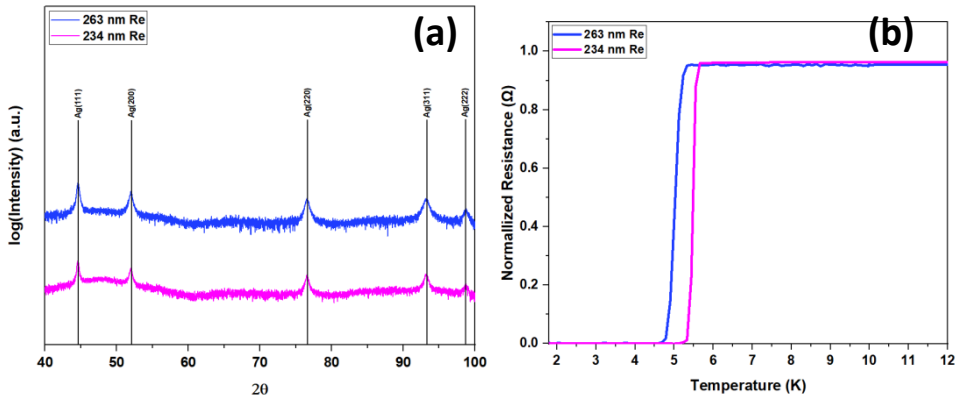

Figure 19. (a) XRD patterns and (b) superconducting transition of two Re films pulse electrodeposited on Ag printed on smooth Kapton.

As discussed earlier, the use of AJP Au seed in replacement of Ag significantly improves the adhesion. As shown in Figure 15, Re electrodeposited on Au is entirely attached to Kapton, both smooth and roughened. Here, the characterization of two typical Re films deposited on Au are presented. Both films are deposited using the typical process, -1 V for 300 seconds at 400 rpm. One sample is on smooth Kapton, the other on Kapton roughened with 1200 grit sandpaper. Figure 20 shows the XRD patterns and the topdown SEM images of these two films. Both films are amorphous with only Au sharp peaks and broad Re peak observed. The top surface of deposited Re showed flat islands with an extremely smooth background. It is not entirely clear what these islands are. It would be surprising if they are Re nucleus because this would suggest a Stranski-Krastanov growth mode, where the film forms island after a 2D layer-by-layer growth.

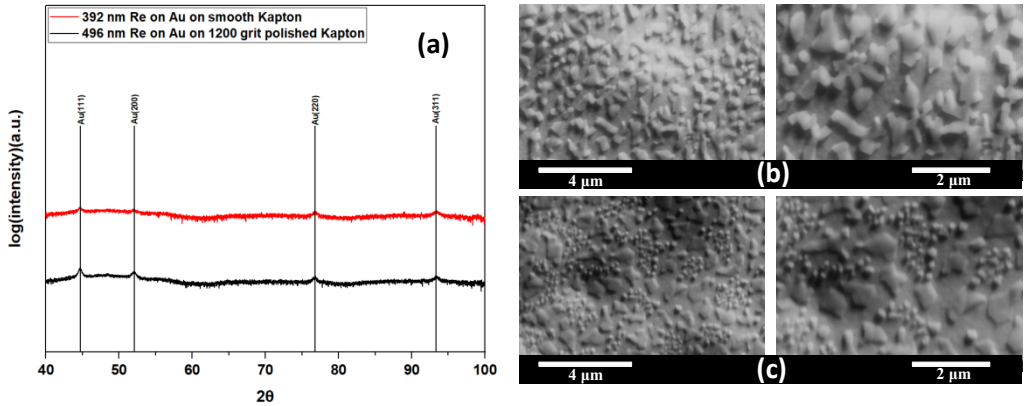

Figure 20. (a) XRD and topdown SEM images of (b) 392 nm and (c) 496 nm Re films electrodeposited on Au printed on (b) smooth Kapton and (c) Kapton roughened with 1200 grit sandpaper.

Further microscopic analysis with EDS elemental mapping was carried out to determine if these islands are metal or oxides. It is worth noting that these films appear metallic silver in color despite

the presence of particles or islands on the surface observed in SEM. Figure 21 shows the results for these two films. The contrast of the elemental maps has been adjusted for better observation of patterns. Re and Au are uniformly distributed with no obvious patterns. On the other hand, the islands observed on SEM correlate extremely well with oxygen signal contrast, suggesting that the islands are certain types of oxides, e.g. Re oxides. It known that surface topography can contribute to signal intensity variation and requires future work to better understand at what condition and how fast such oxides form, and what oxide they are. More discussions on Re film oxidation or film degradation will be provided later.

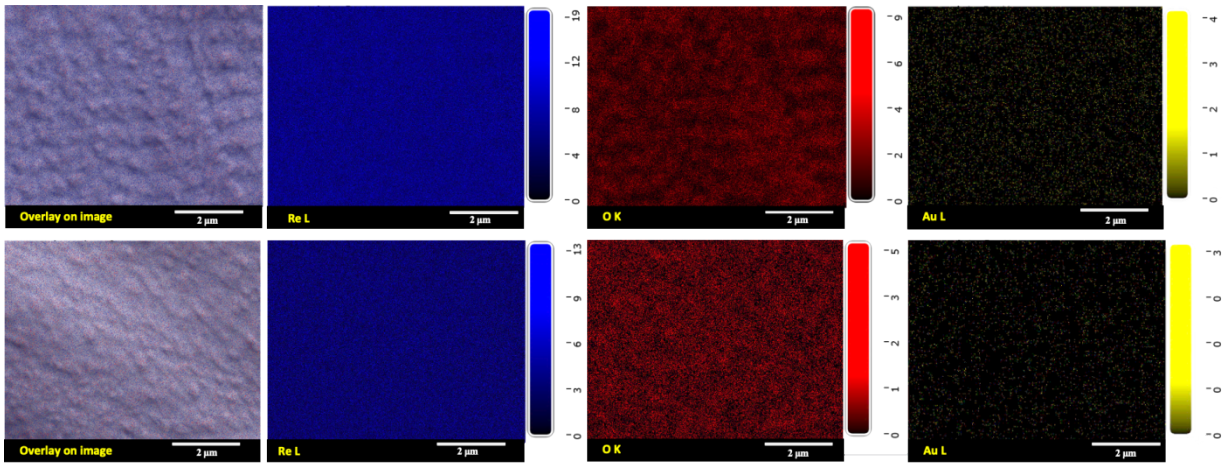

Figure 21. SEM and the Re, O, Au elemental mapping of (top row) 392 nm Re films electrodeposited on Au printed on smooth Kapton; and (bottom row) 496 nm Re films electrodeposited on Au printed on Kapton roughened with 1200 grit sandpaper. The contrasts of the elemental maps have been adjusted for better observation to eyes.

Despite of the formation of oxide islands, the superconducting transition behavior seems to be little impacted. The same two films shown in Figures 20 and 21 are characterized in PPMS for sheet resistance with temperature sweep. As shown in Figure 22(a), a very sharp transition is observed between 6.2 and 6.0 K. Compared with the films on Ag in Figure 18 and 19, these two films are thicker. The slightly higher Tc and sharp transition observed here are consistent with the previous reports for Re deposited on PVD Au on Si [19,15]. In addition to these two films, multiple Re films are deposited in the same condition on Au printed on roughened Kapton. The resistance measurement is repeated and is shown in Figure 22(b). All films showed sharp rapid transitions between 5.8 to 6.1 K. These results demonstrate the good reproducibility of the improved superconductivity of electrodeposited Re on AJP Au seed.

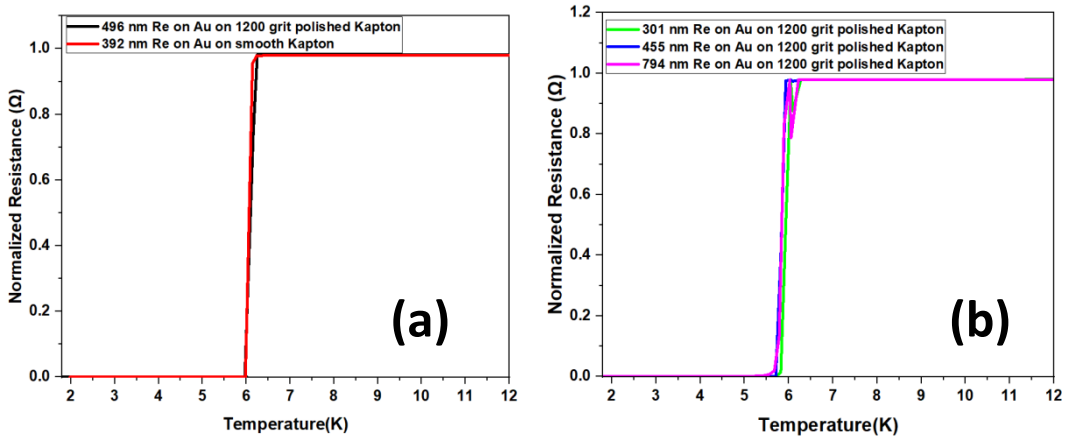

Figure 22. Superconducting transition of (a) the two Re films deposited on Au on roughened and smooth Kapton, and (b) three additional Re films deposited on Au on 1200 grit roughened Kapton.

Flexure Testing

Three point bending testing was used to evaluate the flexure properties of Ag and Au seed layers on 127 µm Kapton films with and without 1200 grit polishing. First, the flexure properties of the bare substrates were tested to establish a baseline for the behavior of these substrates. For bare substrates, three samples as received were tested to 4.5% strain and three samples after polishing to 1200 grit were tested to 3.75% strain as shown in Figure 23. The results show that polishing of the Kapton is correlated with lowered flexibility. At 2% strain where the curve peaks, the unmodified Kapton samples reach a stress of 20 MPa while the 1200 grit polished Kapton samples reach a stress of 30-35 MPa. This would indicate that polishing introduces defects into the film that block the deformation of the Kapton film.

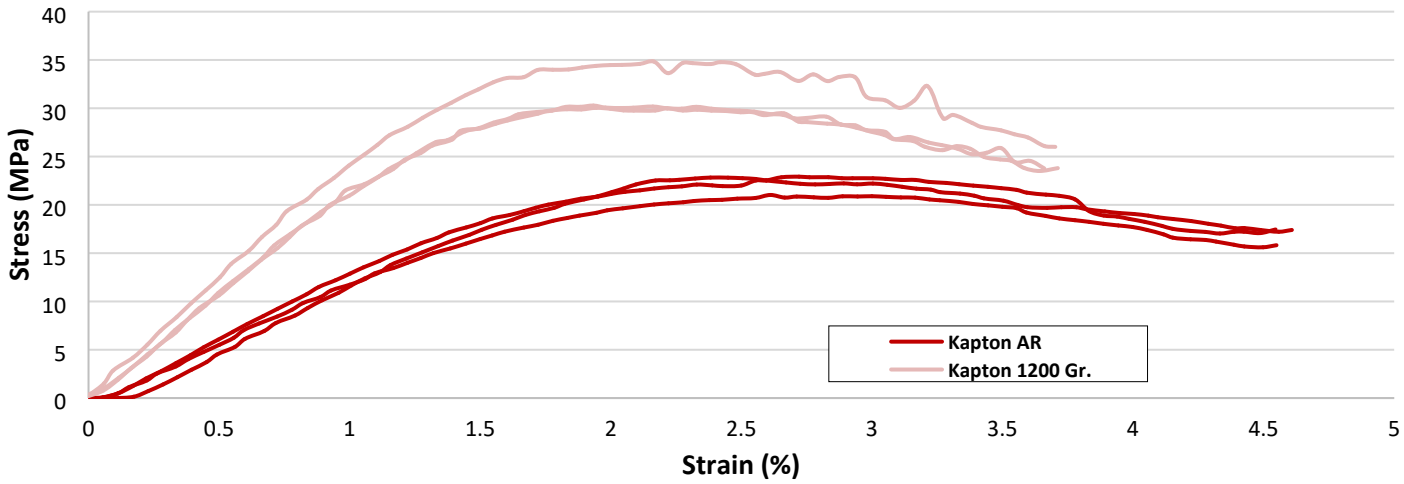

Figure 23. Three-point bend flexure testing of three 127 µm Kapton substrates without Ag or Au printed seed layers. AR indicates Kapton substrates used as received without sandpaper modification while 1200 Gr. indicates Kapton substrates polished to 1200 grit sandpaper.

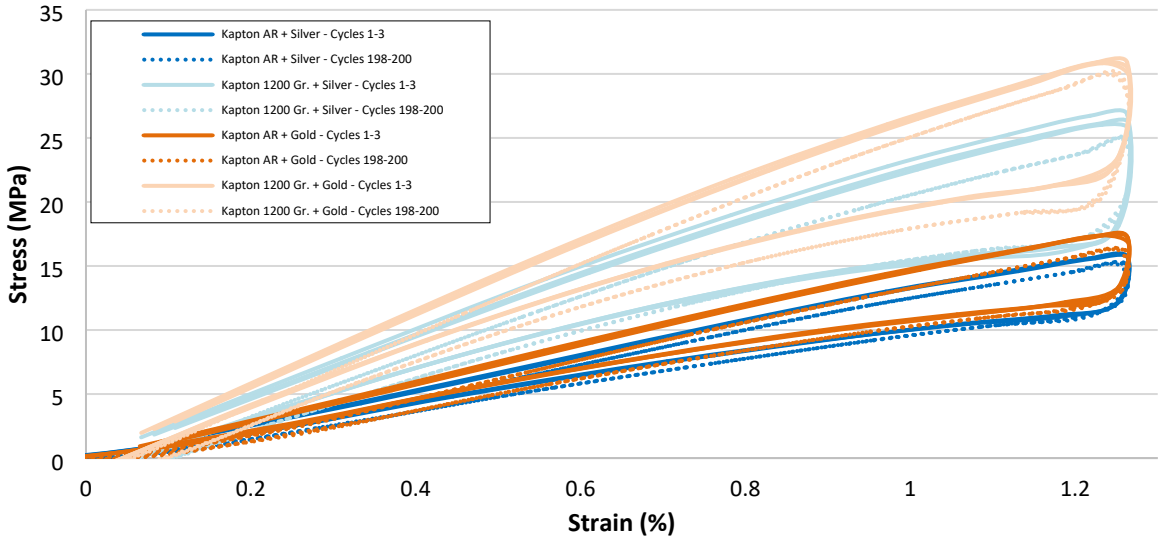

Figure 24. Three-point bend cycling flexure testing of printed Au and Ag on 127 µm Kapton substrates. AR indicates Kapton substrates used as received without sandpaper modification while 1200 Gr. indicates Kapton substrates polished to 1200 grit sandpaper.

Cycling testing of Kapton substrates with Au and Ag were characterized with a strain rate of 0.1/minute, applied for 200 cycles to 1.25% strain and the stress was measured. The results for the first and last 3 cycles are shown in Figure 24. The unpolished films reach a lower stress of 15-17 MPa at 1.25% strain while the roughened samples reached a maximum stress of 27-30 MPa. These values match the results in the bare substrates shown in Figure 23 and indicate that the flexural properties of the substrates dominate over the presence of the AJP seed layer. Profilometry measurements showed that the thickness of printed films is < 5 µm, which is much thinner compared with the 127 µm thickness of the film, so it is reasonable that the substrate's flexibility dominates. A less than 1 MPa shift downward in stress at 1.25% strain is observed between the first 3 cycles and last 3 cycles. No apparent delamination of the printed seed layers was observed.

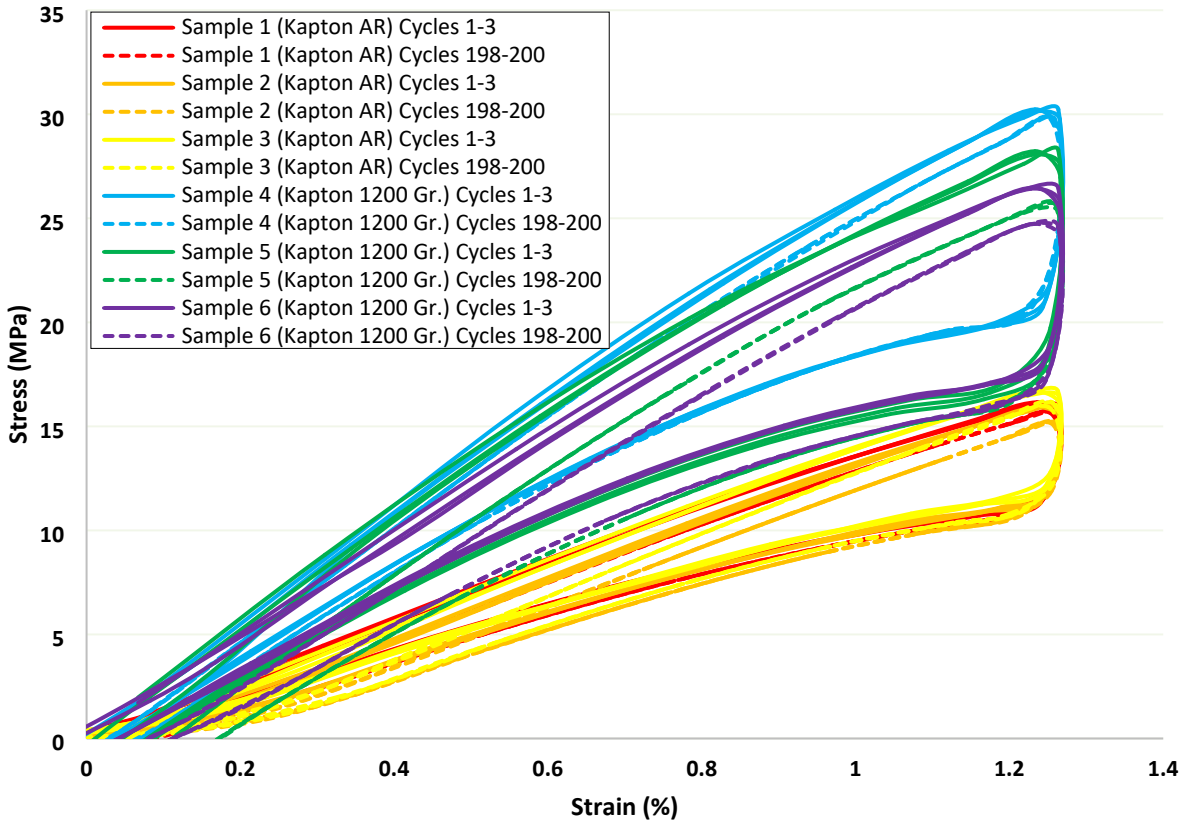

Figure 25. Cycling testing of electrodeposited Re on printed Au seed layers on Kapton substrates. AR indicates Kapton substrates used as received without sandpaper modification while 1200 Gr. indicates Kapton substrates polished to 1200 grit sandpaper.

Figure 25 shows the cycling testing of electrodeposited Re on printed Au on Kapton substrates. Three samples on unmodified (AR) Kapton and three samples of 1200 grit sandpaper roughened Kapton were tested with cyclic three-point bending for 200 cycles to a strain of 1.25%. The results are consistent with the data obtained with cyclic testing on the samples without electrodeposited Re. A maximum stress of 15 MPa at 1.25% was recorded for the unmodified Kapton substrate samples while a maximum stress of 26-30 MPA was recorded for the 1200 grit sandpaper modified samples. These results indicate that the addition of Re has no observable effect on the flexure properties of these samples.

Superconductivity of ECD Re post flexure testing

The effect of repetitive flexure on the superconductivity of the ECD Re is one of the critical questions regarding the reliability of superconducting flexible cable. The rationale behind this concern comes from the observation that the Tc of electrodeposited Re significantly deteriorates upon thermal annealing. This has been related to the grain coarsening of the as-deposit amorphous Re. Mechanical stress can expedite grain growth or induce strains in the film [22-26], which, if occurs to the electrodeposited Re, is expected to impact the Tc. While this subject would require detailed studies in future, the same Re strips undergoing the 200 cycles of bending test are attempted for the Tc measurement. However, the films were found to have degraded. Figures 26 (a) and (b) show an example of the Re film after shipping from UA to Sandia, flexure testing at Sandia, and shipping from Sandia back to UA, which includes aging at ambient condition. Surprisingly, the film has completely turned into black and disintegrated. A sheet resistance measurement is performed on this film using PPMS and no superconducting transition was observed since the film is not metallic Re anymore.

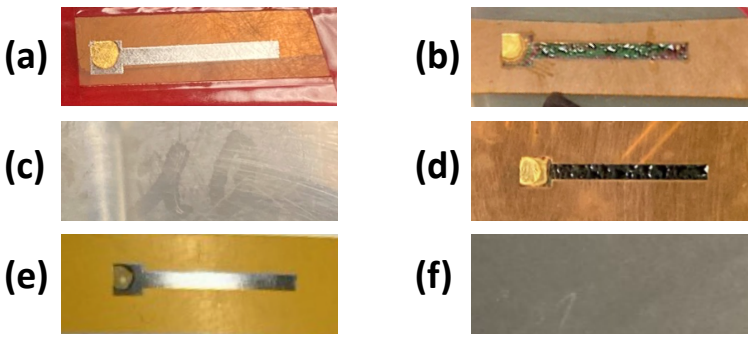

Figure 26. Photos of (a) as deposited Re films on Au AJ printed on Kapton, and (b) the Re film after shipping, handling, and flexure testing. Partition experiments where two duplicate Re films deposited on Au have been aged (c,d) in ambient and (e,f) in a vacuum desiccator for (c,e) 1 day and (d,f) 1 week.

Partitioning experiments are performed to determine the condition for film degradation. In one study, two duplicate Re films are deposited using the same process. One is stored in ambient and one is stored in a vacuum desiccator. The films are inspected after 1 day and 1 week. As shown

in Figures 26 (c) and (d), the film stored in ambient showed some dullness after only one day and turns into completely black after 1 week. On the other hand, as shown in Figures 26 (e) and (f), the same Re film stored in vacuum desiccator did not show any sign of degradation after 1 day or 1 week.

It is not clear what exactly causes the degradation as this degradation has not been observed 100% of time. For example, earlier films survived the shipping from UA to Sandia and retained the silver color. But more recent films shipped in July did not survive and turned black. There has been some indication that such degradation can be accelerated in humid and hot ambient, depending on the shipping. More studies have been conducted to explore a more rigorous cleaning strategy after electrodeposition to better remove chemicals, low temperature thermal annealing process to better ensure the moisture free status of the films before shipment, as well as better packaging to ensure an inert ambient during transition. Investigation into mitigation strategies are underway, results are currently not available.

ANTICIPATED OUTCOMES AND IMPACTS:

Future work will drive to advance the TRL of this work. We will seek to understand and eliminate film degradation for device purposes by improving the stability and reliability. One possible promoter of such degradation could be the AJP Au seed metal, which is an extremely inert metal, yet tends to form a galvanostatic corrosion cell with any other metals when moisture and oxygen is present. Future strategy will include not only the elimination of moisture and oxygen, but also explore capping materials to prevent the moisture and oxygen reaching Re film and provide a cathodic protection for the Re film. We will evaluate low temperature thermal annealing as a process to better ensure the moisture free status of the films. We would like to investigate if cyclic bend testing influences the resistance of the composite or the superconducting transition temperature. This is one of the critical questions surrounding the reliability of superconducting flexible cable and is based on the understanding that grain coarsening of as-deposit amorphous Re leads to a decrease in Tc. We would like to evaluate if grain coarsening occurs from bend testing and if so to what extent. Our results with SEM imaging of Re on Au, on smooth and roughened Kapton showed the formation of oxide islands on a completely smooth background. We would like to better understand at what condition and how fast such oxides form, and what oxide they are. An investigation into different designs and dimensions is of interest as this changes electrical properties such as impedance and frequency response. We would like to evaluate and optimize the printed-deposited structure as a part of future efforts. Through findings in this EE work we identified Au as a having superior adhesion to Kapton over Ag. We would like to understand why Au shows better adhesion and identify a means to lower the cost while maintaining good adhesion.

Presentations and Publications

1. Electrodeposition of Rhenium on AJP Metal Seed Layers on Flexible Substrates, ECS, Fall 2022
2. Invited: Chemistry Effects on the Electrodeposition of Re, Co, and Alloys, ECS, Fall 2022, Prof. Qiang Huang
3. Electrodeposition of Rhenium on Aerosol Jet Printed Metal Seed Layers on a Flexible Substrate" submitting to IEEE or ECS journal

Intellectual Property

- TA: Improved Adhesion of EDC Rhenium on AJP Gold SD# 16172
- Patent application: Submitted by UA, under review September 2022We have formed a strong collaboration with Prof. Qiang Huang at the University of Alabama

The recent results of this project will be shown to Sandia groups working in superconducting systems. Our university collaborator will leverage these results in proposals. Prof. Huang has spoken to SeeQC based in NY as potential industry partners.

This project supports two elements of our division strategy: (1) Nuclear Deterrence- it strengthens our expertise in aerosol jet printing and electrodeposition for electronic interconnections that can be used for integration of microelectronics, (2) Strategic Partnership Program - it advances technology for interconnects for superconducting quantum qubits, supporting building hybrid quantum information systems. To continue to support our division strategy *we will be submitting a full LDRD* proposal in collaboration with UA for FY24 funding cycle. We hope to have the opportunity to leverage this work, answer questions that we did not have resources to address and increase the scope and detail of the work.

CONCLUSION:

The compatibility of aerosol jet printing a metal seed layer with the electrodeposition of Re on Kapton was found to be a viable means to producing flexible superconducting film, however, is dependent upon the metal used as the seed layer. Initial efforts focused on silver as the seed metal because of its relatively high conductivity and low cost. Despite our efforts with silver, which were limited due to the time constraints of this project, we were unable to demonstrate a robust and reliable superconducting Re-Ag-Kapton composite film. We were very successful in this demonstration with gold as the seed metal. Rhenium was electrodeposited from a superhigh concentration of water-in-salt electrolyte on to aerosol jet printed Au seed layer on Kapton with excellent reproducibility. A sharp superconducting transition between 5.8 K and 6.2 K depending on the Kapton surface roughness was measured, establishing this composite film stack as a high performing, low cost, light, flexible and modular superconducting alternate to the current state-

of- the-art. Cyclic bend testing of 200 cycles demonstrated the robustness of the composite film. Cyclic flexure testing to 1.25% strain showed the smooth samples reach a lower stress of ~16 MPa, sandpaper roughened requires ~20MPa. The bend tests also indicate that the addition of Au and Re has no observable effect on the mechanical properties of the samples and the properties are dictated by the substrate. Surface oxidation of electrodeposited rhenium presented itself late in this project which we believe coincided with the increased atmospheric moisture in NM. Further research is needed to mitigate this recent setback. We believe it can be readily resolved by a more controlled environment, use of a capping agent, controlled gentle annealing or some combination of these approaches. In addition, we would like to understand the adhesion differences between gold and silver at the Kapton interface. Finally, we hope to investigate the effect of different designs and dimensions on electrical properties such as impedance and frequency response.

REFERENCES:

1. F. Bova, A. Goldfarb, R.G. Melko “Commercial Applications of Quantum Computing.” *EPJ Quantum Tech.* (2021) 8, 2.
2. V. Hassija, V. Chamola, A. Goyal, S. S. Kanhere, N. Guizani “Forthcoming applications of quantum computing: peeking into the future” *IET Quantum Comm*. (2022), 1, 2, 35-41.
3. Y. Cao, J. Romero, J. P. Olson, M. Degroote, P. D. Johnson, M. Kieferova, I. D. Kivlichan, T. Menke, B. Peropadre, N. P. D. Sawaya, S. Sim, L. Veis, A. Aspuru-Guzik. “Quantum Chemistry in the Age of Quantum Computing.” *Chem. Rev.* (2019), 119, 19, 10856-10915.
4. A. Kumar and S. Garhwal “State-of-the-Art Survey of Quantum Cryptography.” *Archives Comp. Meth. Engr.* (2021) 28, 3831-3868.
5. R. Orus, S. Mugel, E. Lizaso. “Quantum computing for finance: overview and prospects.” *Rev. Phys*. (2019), 4, 100028.
6. S. Krinner, S. Storz, P. Kurpiers, P. Magnard, J. Heinsoo, R. Keller, J. Lütolf, C. Eichler & A. Wallraff. “Engineering cryogenic setups for 100-qubit scale superconducting circuit systems.” *EPJ Quantum Tech*. (2019) 6:2.
7. J. Li, et al. “Printable two-dimensional superconducting monolayer.” Nat. Mater., 2021, 20, 181-187.
8. L. Ren, J. Zhuang, G. Casillas, H. Feng, Y. Liu, X. Xu, Y. Liu, J. Chen, Y. Du, L. Jiang, S. X. Dou, “Nanodroplets for Stretchable Superconducting Circuits.” *Adv. Func. Mater*. 2016, 26, 44, 8111-8118.
9. D. B. Tuckerman, M. C. Hamilton, D. J. Reilly, R. Bai, G. A. Hernandez, J. M. Hornibrook, J. A. Sellers, C. D. Ellis. “Flexible superconducting Nb. Transmission lines on thin film polyimide for quantum computing applications.” *Supercond. Sci. Technol.* 2016, 29, 84007.
10. V. Solovyov, O-P. Saira, Z. Mendleson, I. Drozdov. “YBCO-on-Kapton: Material for High Density Quantum Computer Interconnects with Ultra-Low Thermal Loss.” *IEEE Trans. Appl. Supercond.* 2021, 31, 5, 1700105.
11. N. J. Wilkinson, M. A. A. Smith, R. W. Kay, R. A. Harris. “A review of aerosol jet printing – a non-traditional hybrid process for micro-manufacturing.” *Int. J. Adv. Manuf. Tech*., 2019, 105, 4599-4619.

12. T. P. Moffat and H. Yang, “Patterned Metal Electrodeposition Using an Alkanethiolate Mask.” *J. Electrochem. Soc.*, 1995, 142, L220.
13. Q.-B. Wu, T. A. Green, and S. Roy, “Electrodeposition of microstructures using a patterned anode.” *Electrochemistry Communications*, 2011, 13, 1229–1232.
14. L. K. Tsui, S. C. Kayser, S. A. Strong, and J. M. Lavin, “High Resolution Aerosol Jet Printed Components with Electrodeposition-Enhanced Conductance.” *ECS J. Solid State Sci. Tech*. (2021). 10, 047001.
15. W. D. Sides, E. Hassani, D. P. Pappas, Y. Hu, T. S. Oh, Q. Huang “Grain growth and superconductivity of rhenium electrodeposited from water-in-salt electrolytes.” *J. App. Phys*. (2020). 127, 085301.
16. R.M. Morais, M.S. Klem, M.S. Ozório, T.C. Gomes, and N. Alves, Roughness influence on the sheet resistance of the PEDOT: PSS printed on paper, Current Applied Physics, 18(2), 254, 2018.
17. D. Zhao, T. Liu, J.G. Park, M. Zhang, J.-M. Chen, and B. Wang, Conductivity enhancement of aerosol-jet printed electronics by using silver nanoparticles ink with carbon nanotubes, Microelectronic Engineering, 96, 71, 2012.
18. A. Mahajan, C.D. Frisbie, and L.F. Francis, *Optimization of aerosol jet printing for high-resolution, high-aspect ratio silver lines,* ACS applied materials & interfaces, 5(11), 4856, 2013.
19. Q. Huang and Y. Hu, *Electrodeposition of Superconducting Rhenium with Water-in-Salt Electrolyte,* Journal of The Electrochemical Society, 165(16), D796, 2018.
20. S. De, W.D. Sides, T. Brusuelas, and Q. Huang, Electrodeposition of Superconducting Rhenium-Cobalt Alloys from Water-in-Salt Electrolytes, Journal of Electroanalytical Chemistry, 860, 113889, 2020.
21. B. Malekpouri, K. Ahammed, and Q. Huang, *Electrodeposition and superconductivity of rhenium-iron alloy films from water-in-salt electrolytes,* Journal of Alloys and Compounds, 912, 165077, 2022.
22. S. Brandstetter, K. Zhang, A. Escuadro, J. Weertman, and H. Van Swygenhoven, Grain coarsening during compression of bulk nanocrystalline nickel and copper, Scripta Materialia, 58(1), 61, 2008.
23. R.A. Meirom, D.H. Alsem, A.L. Romasco, T. Clark, R.G. Polcawich, J.S. Pulskamp, M. Dubey, R.O. Ritchie, and C.L. Muhlstein, Fatigue-induced grain coarsening in nanocrystalline platinum films, Acta Materialia, 59(3), 1141, 2011.
24. W. Chen, Z. You, N. Tao, Z. Jin, and L. Lu, Mechanically-induced grain coarsening in gradient nano-grained copper, Acta Materialia, 125, 255, 2017.
25. J. Long, Q. Pan, N. Tao, and L. Lu, *Abnormal grain coarsening in cyclically deformed gradient nanograined Cu,* Scripta Materialia, 145, 99, 2018.
26. O. Glushko and G. Dehm, *Initiation and stagnation of room temperature grain coarsening in cyclically strained gold films,* Acta Materialia, 169, 99, 2019.

LABORATORY DIRECTED RESEARCH & DEVELOPMENT

WHERE INNOVATION BEGINS

ADDENDUM:

Development of Quantum Computing Interconnect Based on Aerosol Jet Printing and Electrochemical Deposition of Rhenium, SD# 227334

Judi Lavin (5219), Qiang Huang (UA), Luke Tsui, Kamal Ahammed (UA), Emily Weigel. Manager: Keith

Purpose: NNSA, Mission Priority 5- Infrastructure Modernization, CC Initiative 5- IT and Cybersecurity: "deliver a modern, secure computing environment that improves communication"; "emerging technologies will be identified/analyzed to strengthen NNSA's cyber defenses" and the *development of novel materials less susceptible to noise and defects*

Current State of the Art: connectors/cables are made from coaxial stainless steel, which require manual assembly of numerous individual cables and result in significant joule heating during operation

Hypothesis: Electrodeposited Re on AJP metal seed layer on Kapton will yield light, flexible, robust films with superconducting properties with high Tc.

Goal and Approach: address limitations in current manufacturing of quantum computing connector cables by the electrodeposition of superconducting rhenium on an aerosol jet printed (AJP) metal seed layer on flexible Kapton substrates

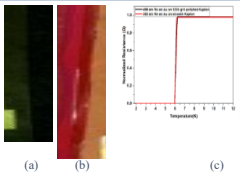

(a) (b) (c)

(a) AJP Au on Kapton (b) Re electrodeposited on Au (c) Superconducting Tc of Re on Au at 6.1 K

R&D Summary

- Integrated AJP of Au and Ag with electrodeposition of Re
- Au on Kapton and Au-Re on Kapton passed ASTM adhesion tests
- Showed an improved and sharp Tc at 6.2 K, above bp of liquid helium (4.2 K)
- Characterized composite by SEM/EDS giving insight into interfacial interaction
- Flexure testing and electrical testing demonstrated robustness and reliability

The result for the one key goal

Electrodeposition of rhenium on AJP gold on Kapton is compatible and a viable approach for flexible connectors however AJP Ag presented adhesion problems

Lessons learned

Must always have alternates or backups for materials and approaches; identify roadblocks as early as possible

Follow-on plans/activities

Hit go, will be submitting a full LDRD collaborative proposal for FY24 funding cycle

Impact of follow-on plans

Get help from your PM if necessary: more details on how this R&D impacts which areas at Sandia

Publications, awards, staff development & IP

Electrodeposition of Rhenium on AJP Metal Seed Layers on Flexible Substrates, EC Fall 2022. Invited: Chemistry Effects on the Electrodeposition of Re, Co, and Alloys ECS, Fall 2022, Prof. Qiang Huang. Electrodeposition of Rhenium on Aerosol Jet Printed Metal Seed Layers on a Flexible Substrate" submitting to IEEE/ECS.
Student intern (Emily Weigel) supported EE with profilometry measurements last week hired on as a technologist in 5219.
TA: Improved Adhesion of EDC Rhenium on AJP Gold SD# 16172
Patent application: Submitted by UA, under review September 2022

LABORATORY DIRECTED
RESEARCH & DEVELOPMENT
WHERE INNOVATION BEGINS

Current Technology, Our Contributions, Metrics & Risk Buy Down

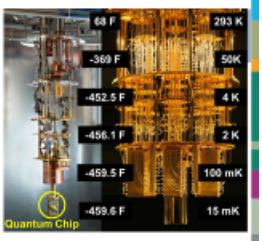

Current State- of-the-Art: Connectors/cables are made from co-axial stainless steel, which require manual assembly of numerous individual cables and result in significant joule heating during operation. QC operates at cryogenic temperatures and performance can only accommodate micro-watt levels of Joule heating. This low tolerance drives design complexity.

Our Contributions: We successfully demonstrated a simple, flexible, light, zero-resistance alternative to current interconnects with quantum chips through the union of AJP and Rhenium electrodeposition on Kapton. The investigated system presents the beginnings of a manufacturable alternative approach to rigid connectors and seeks to mitigate joule heating, temperature perturbations and thermal noise associated with the current state of the art based on our material choice and deposition approach.

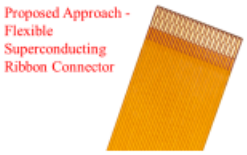

Achieved our go/no go metric: Demonstrated Re electrodeposition on Ag and Au seed layers; Au-Re composite maintained excellent adhesion on Kapton

Risk Buy Down for Future Programs:

- Demonstrated low cost manufacturing for connector cables in quantum computing design
- Shown material compatibility of Au and Re
- Found Au-Re composite to have strong adhesion to Kapton
- Materials were able to withstand 200 cycles of bend testing
- Gained insight into interfacial interactions through SEM/EDS

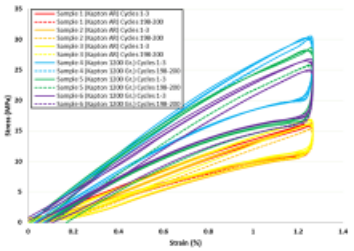

Development of Quantum Computing Interconnect Based on Aerosol Jet Printing and Electrochemical Deposition of Rhenium

We successfully demonstrated the electrodeposition of Rhenium onto AJP Au on flexible Kapton substrates with good reproducibility and demonstrated improved superconductivity with a sharp transition temperature (Tc) between 6.0 and 6.2 K. This establishes the materials and approach evaluated as a low cost, flexible, light and high performing superconducting alternative to current state of the art.

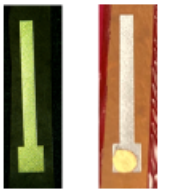

As a team we achieved *all* of our goals in the project plan!

- Integrated AJP of Au and Ag with electrodeposition of Re
- Able to quickly pivot to alternate seed material and successfully develop a reproducible approach to forming a Au-Re composite on flexible Kapton
- Au on Kapton and Au-Re on Kapton passed ASTM adhesion tests
- Showed an improved and sharp Tc at 6.2 K and 6.0 K well above the bp of liquid helium (4.2 K)
- Characterized composite by SEM-EDS giving insight into interfacial interactions
- Flexure testing and electrical testing demonstrated mechanical robustness and superconducting performance

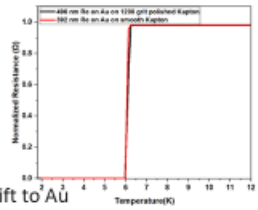

Challenges:

- Ag was the choice seed metal for AJP however poor adhesion of Ag-Re composite to Kapton required us to shift to Au as seed layer (explored means to promote adhesion including surface roughening and pulse electrodeposition)
- The oxidation of Re over time just recently (last couple of weeks) became apparent. Exploring means to stabilize the surface by handling/packaging in an inert environment, evaluating annealing temperatures to drive off moisture (50°C or 70°C/24 hrs) and the electrodeposition of protective layer. Research is still underway; this is an area we hope to investigate further through a full LDRD project

LABORATORY DIRECTED
RESEARCH & DEVELOPMENT
WHERE INNOVATION BEGINS

Summary of Results

- Work involved the union of two techniques –aerosol printing and Rhenium electrodeposition – that had not been demonstrated in the literature. Initial efforts focused on Ag as the seed metal layer
- Evaluated different gauges of Kapton and surface roughness (using different grits of sandpaper)
- Adhesion of Ag on Kapton was good, however upon Re deposition significant stress developed, delamination occurred. Efforts to reduce stress using pulse electrodeposition did lower the overall stress, but partial delamination still occurred.
- Moved to Au as seed layer – strong adhesion to Kapton and of Au-Re composite to Kapton (both smooth & roughened)
- XRD showed sharp peaks for only Au and Re remains amorphous; SEM showed flat islands with smooth background; EDS elemental mapping correlated the islands with oxygen, potentially Re-oxide
- Au-Re on Kapton reproducibly showed superconducting transition between 5.8 and 6.2 K on smooth and roughened Kapton respectively (thickness dependent)
- Cyclic flexure testing to 1.25% strain showed the smooth samples reach a lower stress of ~16 MPa, sandpaper roughened reached a stress ~20MPa
- Flexure results showed the addition of Re and Au has no observable effect on the mechanical properties of the samples

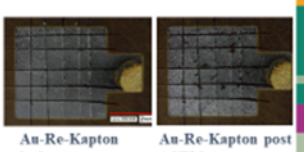

Au-Re-Kapton before tape test | Au-Re-Kapton post ASTM tape test

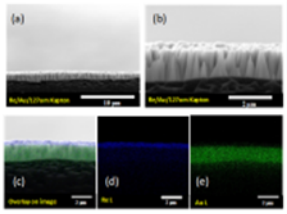

(a,b) SEM images, (c,d,e) EDS elemental mapping of an inner cross section of Re on AJP Au on Kapton

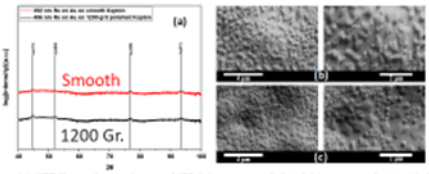

(a) XRD and topdown SEM images of (b) 392 nm and (c) 496 nm Re films electrodeposited on Au printed on (b) smooth Kapton and (c) Kapton roughened with 1200 grit sandpaper.

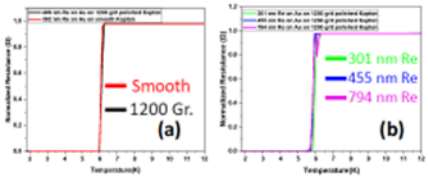

Superconducting transition of (a) the two Re films deposited on Au on roughened and smooth Kapton, and (b) three additional Re films of varying thicknesses deposited on Au on 1200 grit roughened Kapton.

LDRD Project Metrics

Presentations and Publications

- Electrodeposition of Rhenium on AJP Metal Seed Layers on Flexible Substrates, ECS, Fall 2022
- Invited: Chemistry Effects on the Electrodeposition of Re, Co, and Alloys, ECS, Fall 2022, Prof. Qiang Huang
- "Electrodeposition of Rhenium on Aerosol Jet Printed Metal Seed Layers on a Flexible Substrate" submitting to IEEE or ECS journal

Intellectual Property

- TA: Improved Adhesion of ECD Rhenium on AJP Gold SD# 16172
- Patent application: Submitted by UA, under review September, 2022

Tools and Capabilities

- Developed a process for stress-strain testing of seed metal and composite on Kapton with colleagues in 1850

Staff Development

- Established a very strong and productive collaborative relationship with Prof. Huang at UA through this EE
- Graduate student (Kamal Ahammed) from UA worked heavily on this project. Student intern (Emily Weigel) supported this work with profilometry measurements, was hired on as a technologist in 5219 two weeks ago. Technologist (Shianne Carroll) <5 years at SNL supported work with bend testing. Post-doc (Yongkun Sui) was supportive throughout project.

LABORATORY DIRECTED
RESEARCH & DEVELOPMENT
WHERE INNOVATION BEGINS

Project Legacy

Key Technical Accomplishment

Electrodeposition of Rhenium on AJP Au on flexible Kapton substrate, demonstrating a superconducting critical temperature, Tc, of 6.2 K.

Sandia missions

This project supports two elements of our division strategy:

- ND - it strengthens our expertise in aerosol jet printing and electrodeposition for electronic interconnections that can be used for integration of microelectronics
- SPP - it advances technology for interconnects for superconducting quantum qubits, supporting building hybrid quantum information systems
- We have formed a strong collaboration with Prof. Qiang Huang at the University of Alabama
- Collaborated with Org. 1850, Materials Reliability and Aging
- The recent results of this project will be shown to Sandia groups working in superconducting systems
- Our university collaborator will leverage these results in proposals
- Prof. Huang has spoken to SeeQC based in NY as potential industry partners

Plans for follow-on and partnerships?

- Submitting a full LDRD proposal in collaboration with UA for FY24 funding cycle to leverage this work, answer questions that we did not have resources to address and increase the scope and detail of the work

Would like investigate if cyclic bend testing effects the resistance of the composite or the superconducting transition temperature, however due to recent oxidation issues we are unable to present the data at this time.

Hope to investigate the effect of different designs and dimensions on electrical properties such as impedance and frequency response.